Published in final edited form as:

Cell Host Microbe. 2016 October 12; 20(4): 423–428. doi:10.1016/j.chom.2016.09.006.

Zika virus infection induces cranial neural crest cells to produce cytokines at levels detrimental for neurogenesis

Nicholas L. Bayless[1,*], **Rachel S. Greenberg**[2,*], **Tomek Swigut**[2,3], **Joanna Wysocka**[2,3,4,5], and **Catherine A. Blish**[1,6,7]

[1]Stanford Immunology, Stanford School of Medicine, Stanford University, 94305, USA

[2]Department of Developmental Biology, Stanford University School of Medicine, Stanford, CA 94305, USA

[3]Department of Chemical and Systems Biology, Stanford University School of Medicine, Stanford, CA 94305, USA

[4]Howard Hughes Medical Institute, Stanford University School of Medicine, Stanford, CA 94305, USA

[5]Institute of Stem Cell Biology and Regenerative Medicine, Stanford University School of Medicine, Stanford, CA 94305, USA

[6]Department of Medicine, Stanford School of Medicine, Stanford University, Stanford, CA 94305, USA

SUMMARY

Zika virus (ZIKV) infection during pregnancy is linked to microcephaly attributed to infection of developing brain structures. ZIKV infects neural progenitor cells *in vitro,* though its effects on other developmentally relevant stem cell populations, including cranial neural crest cells (CNCCs), have not been assessed. CNCCs give rise to most cranial bones and exert paracrine effects on the developing brain. Here, we report that CNCCs are productively infected by ZIKV, but not by the related dengue virus. ZIKV-infected CNCCs undergo limited apoptosis but secrete cytokines that promote death and drive aberrant differentiation of neural progenitor cultures. Addition of two such cytokines, LIF or VEGF, at levels comparable to those secreted by ZIKV-infected CNCCs is sufficient to recapitulate premature neuronal differentiation and apoptotic death of neural

Corresponding authors: C.A.B., cblish@stanford.edu, J.W. wysocka@stanford.edu.
[7]Lead Contact
[*]Co-first author

SUPPLEMENTAL INFORMATION

Supplemental information associated with this article contains 6 additional figures and supplemental experimental methods.

AUTHOR CONTRIBUTIONS

N.L.B. and R.S.G. designed and performed the experiments, conducted data analysis and wrote the manuscript. T.S. performed data analysis and guided experimental design. J.W. and C.A.B. provided scientific oversight and guidance, edited the manuscript and provided funding for the studies.

progenitors. Thus, our results suggest that CNCC infection by ZIKV may contribute to associated embryopathies through signaling cross-talk between developing face and brain structures.

Graphical Abstract

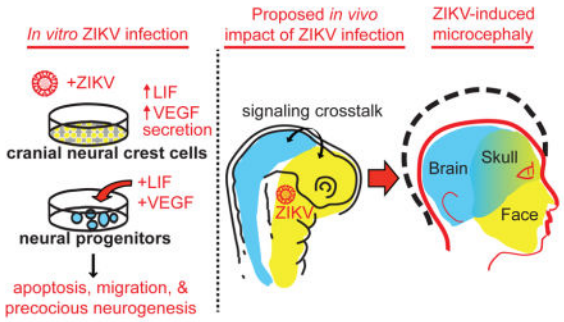

Keywords

Zika virus; microcephaly; neural development; stem cells; cytokines; growth factors

MAIN TEXT

Zika virus (ZIKV), an arbovirus of the *Flaviviridae* family first isolated in Uganda in 1947, has recently undergone a major outbreak in Latin American countries, where it has been linked to significant adverse fetal outcomes including microcephaly (Brasil et al., 2016). A significant effort has subsequently been devoted to defining mechanisms underlying the developmental abnormalities that lead to microcephaly, with the focus on the direct effects of ZIKV infection on growth and survival of the neural progenitor cells (NPCs), whose expansion or decline ultimately affects brain size. These studies demonstrated that ZIKV infects human NPCs and *in vitro* derived brain organoids, impeding their proliferation and survival (Garcez et al., 2016; Tang et al., 2016).

However, brain development is a complex process influenced by the paracrine effects from other surrounding embryonic structures. For example, development of the brain and face is integrated at multiple levels, and this integration is mediated by the spatial proximity, shared inductive pathways and signaling crosstalk between the two developing structures (Marcucio et al., 2015). Consequently, dysfunction in either system can affect the other. Interestingly, in the context of ZIKV-induced microcephaly, the majority of cases are accompanied by craniofacial abnormalities (de Fatima Vasco Aragao et al., 2016), suggesting that such crosstalk may be relevant for understanding the ZIKV-associated embryopathies. Craniofacial structures, including the majority of bone, cartilage, smooth muscle and vasculature of the head and face, are largely derived from a migratory embryonic cell population called cranial neural crest cells (CNCCs). CNCCs emerge from the dorsal-anterior neural tube, and thus share embryonic origins with the developing central nervous system. Later in embryogenesis, as CNCCs form facial structures, the signaling molecules secreted by them are necessary for normal brain development (Le Douarin et al., 2007).

We hypothesized that, in addition to the previously reported direct effects of ZIKV infection on NPCs, this virus can also affect neurogenesis indirectly, via paracrine effects mediated by the infection of CNCCs. To test this hypothesis, we took advantage of the *in vitro* differentiation model previously developed in our lab, in which human embryonic stem cells (hESC) are first induced to form neuroepithelial spheres that subsequently attach and give rise to migratory CNCCs (Bajpai et al., 2010; Prescott et al., 2015) (Figure 1A). *In vitro* derived human CNCCs can be maintained as a nearly homogenous population exhibiting molecular and cellular characteristics of bona fide embryonic CNCCs (Bajpai et al., 2010; Prescott et al., 2015). To test susceptibility of these *in vitro* derived CNCCs to infection, we exposed CNCCs at early (p3) and late (p6) passages to ZIKV and, to facilitate relative comparisons, performed parallel infections of hESCs and neuroepithelial spheres at matched MOI (Figure 1A). Intracellular staining for flavivirus group antigen (which recognizes both ZIKV and the related dengue flavivirus, DENV) followed by flow cytometry analysis revealed that CNCCs were consistently more robustly infected with ZIKV than either hESCs or neuroepithelial spheres (example analysis shown in Figure 1B with % of positively stained cells indicated for each cell population). Confocal imaging of immunostained cells confirmed detection of viral cytoplasmic signal only in ZIKV-infected samples, and expression of canonical CNCC markers p75 and Sox9 in the ZIKV+ cells (Figure S1A). To assess whether CNCCs were permissive to viral reproduction, cellular supernatants were harvested from CNCCs 24 hours following ZIKV infection, and assessed for viral titer by plaque assay on Vero cells (Figure 1C). CNCCs supported a productive infection, with 10^5–10^7 plaque forming units detected in the supernatant at MOIs of 0.01 to 0.1, a concentration that exceeds the concentration of introduced viral particles 2–10-fold. In contrast, DENV at matched MOI failed to infect CNCCs: in a representative experiment, 27.6% of ZIKV-infected CNCCs were positive for flavivirus group antigen by flow cytometry, compared to 0.20% of DENV-infected cells and 0.14% of mock-infected cells (Figure 1D). In all, ZIKV was associated with a significantly increased frequency of flavivirus group antigen positive cells ($p = 0.0078$, Wilcoxon paired signed-rank test) compared to mock infection and to DENV infection ($p = 0.044$, unpaired Mann-Whitney test) (Figure 1E). Consistent with the observed tropism of ZIKV and DENV, RNA-seq analysis reveals that CNCC express AXL, which allows ZIKV entry (Nowakowski et al., 2016; Savidis et al., 2016) at much greater levels than DC-SIGN, a canonical entry receptor for DENV (Cruz-Oliveira et al., 2015), (Figure S1B).

Despite productive infection of CNCCs with ZIKV, relatively little apoptotic death is seen following ZIKV infection. We observe a minor increase in apoptotic death at 24 hours after ZIKV exposure (4.3% compared to 3.6% at baseline), but not for DENV (2.9% compared to 3.6%) (Figure 1F). This effect is slightly more pronounced at 72 hours after exposure, with 8.8% of the ZIKV virus infected cells undergoing apoptotic death, compared to 4% apoptosis with mock infection ant 3.9% with DENV. (Figure 1G). A lower MOI leads to a slight decrease in levels of apoptosis (Figure S1E). Taken together, these observations indicate that CNCCs are highly susceptible to ZIKV infection and support viral replication while only experiencing modest apoptotic death. Interestingly, this susceptibility is specific, as CNCCs are resistant to infection by a related flavivirus, DENV.

In light of the importance of CNCCs in establishing the signaling milieu in the developing brain, we next examined whether the paracrine effects of ZIKV-infected CNCCs could have an effect on developing neural progenitor cells. To this end, CNCC monolayers were seeded on transwell membranes and infected with ZIKV (or mock infected) for 24 hours before co-culturing with neurospheres separated by the transwell membrane. After 3 days, neurospheres were fixed and visualized by confocal immunofluorescence imaging. Migratory projections were visualized as $Tuj1^{+}DAPI^{+}$ protrusions migrating away from the sphere bolus (Figure 1Hi), increased neuronal growth as $Tuj1^{+}$ axonal projections (Figure 1Hii), and apoptosis by cleaved caspase-3 staining (Figure 1H, green). Neurospheres co-incubated in with ZIKV-infected, but not uninfected, CNCCs across a transwell membrane showed striking changes in morphology, including presence of migratory or neuronal projections (Figure 1H, quantified in Figure 1I). Notably, the pronounced morphological differences seen after co-incubation with infected CNCCs are not seen following direct infection of neurospheres with ZIKV (Figure S1F). In addition, apoptosis is significantly increased in neurospheres co-incubated with infected CNCCs, compared to neurospheres cultured alone (Figure 1H, Figure 1J).

To identify the specific soluble factors involved in the paracrine exchange between CNCCs and neural progenitors that drive ZIKV pathogenesis, we harvested cell supernatants from two independent infections of CNCCs for assessment of cytokine concentrations using a human 63-plex Luminex assay (Kuznetsova et al., 2015). Following infection with ZIKV at an MOI of 0.1, CNCCs produced over 60-fold more LIF, IL-6, and PAI-1 and 10-fold more VEGF, IL-17F, TGF-α and MCSF than mock infected controls, and these increases showed dose-dependency on the viral titer (Figure 2A, S2A). Exposure to DENV did not elicit a cytokine response of note (Figure 2B), and the same cytokine profile is elicited by MR-766 or H/PF/2013 strains of ZIKV (Figure 2B, S2F). ZIKV-infected CNCCs secreted LIF at a concentration of 620 pg/mL, compared to 1 pg/ml as seen from the mock infected controls (Figure 2C). Other cytokines secreted at high concentrations included IL-6 (2427 pg/ml in ZIKV vs. 6.78 pg/ml in mock), PAI-1 (3978 pg/ml in ZIKV vs. 38.6 pg/ml in mock), and VEGF (16 ng/ml in ZIKV vs. 0.26 ng/ml in mock) (Figure 2D, Figure S2B–C). Importantly, infection did not universally increase cytokine concentrations; for instance, neither IL-10 (9 pg/ml in ZIKV vs. 8 pg/ml in mock) nor VCAM1 (3.7 ng/ml in ZIKV vs. 2.1 ng/ml in mock) were significantly elevated in response to infection (Figure S2D–E). Of note, we also did not observe a strong interferon response, with less than 2-fold induction of IFN-α, -β, and -γ (Figure 2A), an observation consistent with previously reported requirements for ZIKV replication (Hamel et al., 2015; Lazear et al., 2016).

Our results are in agreement with the possibility that cytokines secreted by ZIKV-infected CNCCs may influence neurogenesis. To test this, we treated hESC-derived neurospheres with LIF or VEGF at concentrations corresponding to those secreted by infected CNCCs. We selected these two cytokines for our proof-of-principle experiments, as they have been previously linked to neural progenitor cell proliferation, neurogenesis and/or neuronal migration, which are processes perturbed in our co-culture experiments (Bauer and Patterson, 2006; Mackenzie and Ruhrberg, 2012; Simamura et al., 2010). In addition, neural progenitors express receptors for both LIF and VEGF, suggesting that in principle, they should be responsive to these signals (Figure S1C–D). After a 3 day treatment, increased

migratory cellular outgrowth and increased neuronal growth were observed in neurospheres developing in the presence of LIF or VEGF (Figure 2E, Figure S2G). Blinded image quantification revealed that untreated neurospheres had a significantly higher frequency of spheres lacking migratory (Figure 2Ei) or neuronal projections (Figure 2Eii) compared to neurospheres treated with either LIF or VEGF (Figure 2F, media vs. LIF, $n = 202$, $p = 0.0029$; media vs. VEGF, $n = 169$, $p < 0.0001$, chi-square test for equal proportionality). Furthermore, spheres treated with either LIF or VEGF had higher proportions of neurospheres with migratory cellular growth compared to untreated spheres (Figure S2H, media vs. LIF, $n = 202$, $p = 0.0289$; media vs. VEGF, $n = 169$, $p = 0.0029$, chi-square test for equal proportionality). Although the proportion of neurospheres that had at least one neuronal outgrowth was not significantly affected between the conditions (Figure S2I), when spheres with >15 neuronal projections were considered, significant differences in neuronal phenotype were observed between untreated and either LIF or VEGF treated cells (Figure 2G, media vs. LIF, $n = 39$, $p = 0.0154$; media vs. VEGF, $n = 36$, $p = 0.0077$, chi-square test for equal proportionality). More detailed analysis uncovered a shift towards a higher number of axonal projections per sphere in LIF or VEGF treated conditions (Figure S2J), with spheres containing >35 projections present only in LIF or VEGF treated samples, but not untreated controls. Both conditions also significantly increased the frequency of apoptotic cell death, as detected by cleaved caspase-3 staining (Figure 2H, LIF vs. media: $p = 0.0152$; VEGF vs. media: $p = 0.0022$, Mann-Whitney test). In sum, these results show that addition of LIF or VEGF at levels elicited by ZIKV in CNCCs to the developing neurospheres results in precocious neurogenesis, increased migration and elevated apoptosis. Importantly, in the *in vivo* context, these phenotypes can contribute to microcephaly, as proliferation, survival, and differentiation timing can all ultimately affect neural progenitor cell numbers and influence brain size.

Our observation that ZIKV causes productive infection in CNCCs is significant on several levels. Firstly, size and development of the skull are affected in ZIKV-associated microcephaly. While this may be an indirect consequence of defective brain growth, in light of our results direct impact of ZIKV infection on cranial mesenchyme should be considered. Secondly, we showed that ZIKV can replicate in CNCCs and that the majority of ZIKV-infected CNCCs do not seem to undergo apoptosis, and thus these cells (and potentially their derivatives) could act as a reservoir for ZIKV reproduction in the vicinity of the developing brain, allowing for continued secretion of infectious virus. Since no infection or viral replication by DENV is seen, the resistance of CNCCs to DENV may provide one explanation of the lack of significant adverse fetal outcomes following maternal DENV infection. Finally, as the development of CNCCs and their derivatives is closely intertwined with the formation of the central nervous system, our data uncovers a potential mechanism by which ZIKV infection may drive embryonic pathogenesis in the brain itself. Considerable increases in secretion of LIF, VEGF, IL-6 and other molecules by ZIKV-infected CNCCs could have both autocrine effects (in turn affecting formation of cranial bone and cartilage) as well as paracrine effects on the developing central nervous system. Indeed, we provide evidence that addition of either LIF or VEGF alone at concentrations elicited by ZIKV infection influences survival and differentiation of neural progenitor cells. Thus, our work

brings attention to previously unappreciated non cell-autonomous mechanisms that may underlie ZIKV-associated microcephaly.

Supplementary Material

Refer to Web version on PubMed Central for supplementary material.

Acknowledgments

We particularly thank Dr. Sara Prescott for her assistance with scoring neurosphere images. We thank Dr. Yael Rosenberg-Hasson in the Stanford Human Immune Monitoring Center for assistance with the Luminex assay. We thank Dr. Michael Diamond for protocols and reagents, Dr. Cécile Baronti for the H/PF/2013 Zika virus strain and Dr. Karim Majzoub for assistance in establishing viral stocks for ZIKV. We thank Bo Gu for assistance with the apoptosis analysis and Dr. Hannah Long for assistance with cell culture. We thank Dr. Laura Simpson and Julia McKechnie for growing DENV stocks. This work was supported by the following funding sources: Tasha and John Morgridge Endowed Faculty Scholar (C.A.B.) in Pediatric Translational Medicine from Stanford Child Health Research Institute and Stanford University School of Medicine, and NIH Director's New Innovator Award to C.A.B. (1DP2AI112193); NIDCR U01 (DE024430), March of Dimes Birth Defects Foundation and Howard Hughes Medical Institute grants to J.W. R.S.G. is supported by a Ruth L. Kirschstein NRSA F31 award from NIDCR (1F31DE025534); N.L.B is supported by the Stanford Graduate Fellowship and a Ruth L. Kirschstein NRSA F31 award from NICHD (1F31HD089675). This work was also supported by a Stanford Systems Biology Seed Grant (2016–2017) to N.L.B. and R.S.G.

References

Bajpai R, Chen DA, Rada-Iglesias A, Zhang J, Xiong Y, Helms J, Chang CP, Zhao Y, Swigut T, Wysocka J. CHD7 cooperates with PBAF to control multipotent neural crest formation. Nature. 2010; 463:958–962. DOI: 10.1038/nature08733 [PubMed: 20130577]

Bauer S, Patterson PH. Leukemia inhibitory factor promotes neural stem cell self-renewal in the adult brain. J Neurosci. 2006; 26:12089–12099. DOI: 10.1523/JNEUROSCI.3047-06.2006 [PubMed: 17108182]

Brasil P, Pereira JP, Raja Gabaglia C, Damasceno L, Wakimoto M, Ribeiro Nogueira RM, Carvalho de Sequeira P, Machado Siqueira A, Abreu de Carvalho LM, Cotrim da Cunha D, Calvet GA, Neves ES, Moreira ME, Rodrigues Baião AE, Nassar de Carvalho PR, Janzen C, Valderramos SG, Cherry JD, Bispo de Filippis AM, Nielsen-Saines K. Zika Virus Infection in Pregnant Women in Rio de Janeiro - Preliminary Report. new england Journal of Medicine. 2016; doi: 10.1056/NEJMoa1602412

Cruz-Oliveira C, Freire JM, Conceição TM, Higa LM, Castanho MARB, Da Poian AT. Receptors and routes of dengue virus entry into the host cells. FEMS Microbiol Rev. 2015; 39:155–170. DOI: 10.1093/femsre/fuu004 [PubMed: 25725010]

de Fatima Vasco Aragao M, van der Linden V, Brainer-Lima AM, Coeli RR, Rocha MA, Sobral da Silva P, Durce Costa Gomes de Carvalho M, van der Linden A, Cesario de Holanda A, Valenca MM. Clinical features and neuroimaging (CT and MRI) findings in presumed Zika virus related congenital infection and microcephaly: retrospective case series study. BMJ. 2016; 353:i1901.doi: 10.1136/bmj.i1901 [PubMed: 27075009]

Garcez PP, Loiola EC, Madeiro da Costa R, Higa LM, Trindade P, Delvecchio R, Nascimento JM, Brindeiro R, Tanuri A, Rehen SK. Zika virus impairs growth in human neurospheres and brain organoids. Science. 2016; 352:816–818. DOI: 10.1126/science.aaf6116 [PubMed: 27064148]

Hamel R, Dejarnac O, Wichit S, Ekchariyawat P, Neyret A, Luplertlop N, Perera-Lecoin M, Surasombatpattana P, Talignani L, Thomas F, Cao-Lormeau VM, Choumet V, Briant L, Desprès P, Amara A, Yssel H, Missé D. Biology of Zika Virus Infection in Human Skin Cells. Journal of Virology. 2015; 89:8880–8896. DOI: 10.1128/JVI.00354-15 [PubMed: 26085147]

Kuznetsova T, Haddad F, Knez J, Rosenberg-Hasson Y, Sung J, Cauwenberghs N, Thijs L, Karakikes I, Maecker H, Mahaffey KW, Wu JC, Staessen JA. Cytokines profile in hypertensive patients with left ventricular remodeling and dysfunction. J Am Soc Hypertens. 2015; 9:975–84. e3. DOI: 10.1016/j.jash.2015.10.003 [PubMed: 26565110]

Lazear HM, Govero J, Smith AM, Platt DJ, Fernandez E, Miner JJ, Diamond MS. A Mouse Model of Zika Virus Pathogenesis. Cell Host & Microbe. 2016; 19:720–730. DOI: 10.1016/j.chom.2016.03.010 [PubMed: 27066744]

Le Douarin NM, Brito JM, Creuzet S. Role of the neural crest in face and brain development. Brain Res Rev. 2007; 55:237–247. DOI: 10.1016/j.brainresrev.2007.06.023 [PubMed: 17765317]

Mackenzie F, Ruhrberg C. Diverse roles for VEGF-A in the nervous system. Development. 2012; 139:1371–1380. DOI: 10.1242/dev.072348 [PubMed: 22434866]

Marcucio R, Hallgrimsson B, Young NM. Facial Morphogenesis: Physical and Molecular Interactions Between the Brain and the Face. Curr Top Dev Biol. 2015; 115:299–320. DOI: 10.1016/bs.ctdb.2015.09.001 [PubMed: 26589930]

Nowakowski TJ, Pollen AA, Di Lullo E, Sandoval-Espinosa C, Bershteyn M, Kriegstein AR. Expression Analysis Highlights AXL as a Candidate Zika Virus Entry Receptor in Neural Stem Cells. Cell Stem Cell. 2016; 18:591–596. DOI: 10.1016/j.stem.2016.03.012 [PubMed: 27038591]

Prescott SL, Srinivasan R, Marchetto MC, Grishina I, Narvaiza I, Selleri L, Gage FH, Swigut T, Wysocka J. Enhancer Divergence and cis-Regulatory Evolution in the Human and Chimp Neural Crest. Cell. 2015; 163:68–83. DOI: 10.1016/j.cell.2015.08.036 [PubMed: 26365491]

Rada-Iglesias A, Bajpai R, Prescott S, Brugmann SA, Swigut T, Wysocka J. Epigenomic annotation of enhancers predicts transcriptional regulators of human neural crest. Cell Stem Cell. 2012; 11:633–648. DOI: 10.1016/j.stem.2012.07.006 [PubMed: 22981823]

Rada-Iglesias A, Bajpai R, Swigut T, Brugmann SA, Flynn RA, Wysocka J. A unique chromatin signature uncovers early developmental enhancers in humans. Nature. 2011; 470:279–283. DOI: 10.1038/nature09692 [PubMed: 21160473]

Savidis G, McDougall WM, Meraner P, Perreira JM, Portmann JM, Trincucci G, John SP, Aker AM, Renzette N, Robbins DR, Guo Z, Green S, Kowalik TF, Brass AL. Identification of Zika Virus and Dengue Virus Dependency Factors using Functional Genomics. Cell Rep. 2016; 16:232–246. DOI: 10.1016/j.celrep.2016.06.028 [PubMed: 27342126]

Simamura E, Shimada H, Higashi N, Uchishiba M, Otani H, Hatta T. Maternal leukemia inhibitory factor (LIF) promotes fetal neurogenesis via a LIF-ACTH-LIF signaling relay pathway. Endocrinology. 2010; 151:1853–1862. DOI: 10.1210/en.2009-0985 [PubMed: 20160138]

Tang H, Hammack C, Ogden SC, Wen Z, Qian X, Li Y, Yao B, Shin J, Zhang F, Lee EM, Christian KM, Didier RA, Jin P, Song H, Ming GL. Zika Virus Infects Human Cortical Neural Progenitors and Attenuates Their Growth. Cell Stem Cell. 2016; 18:587–590. DOI: 10.1016/j.stem.2016.02.016 [PubMed: 26952870]

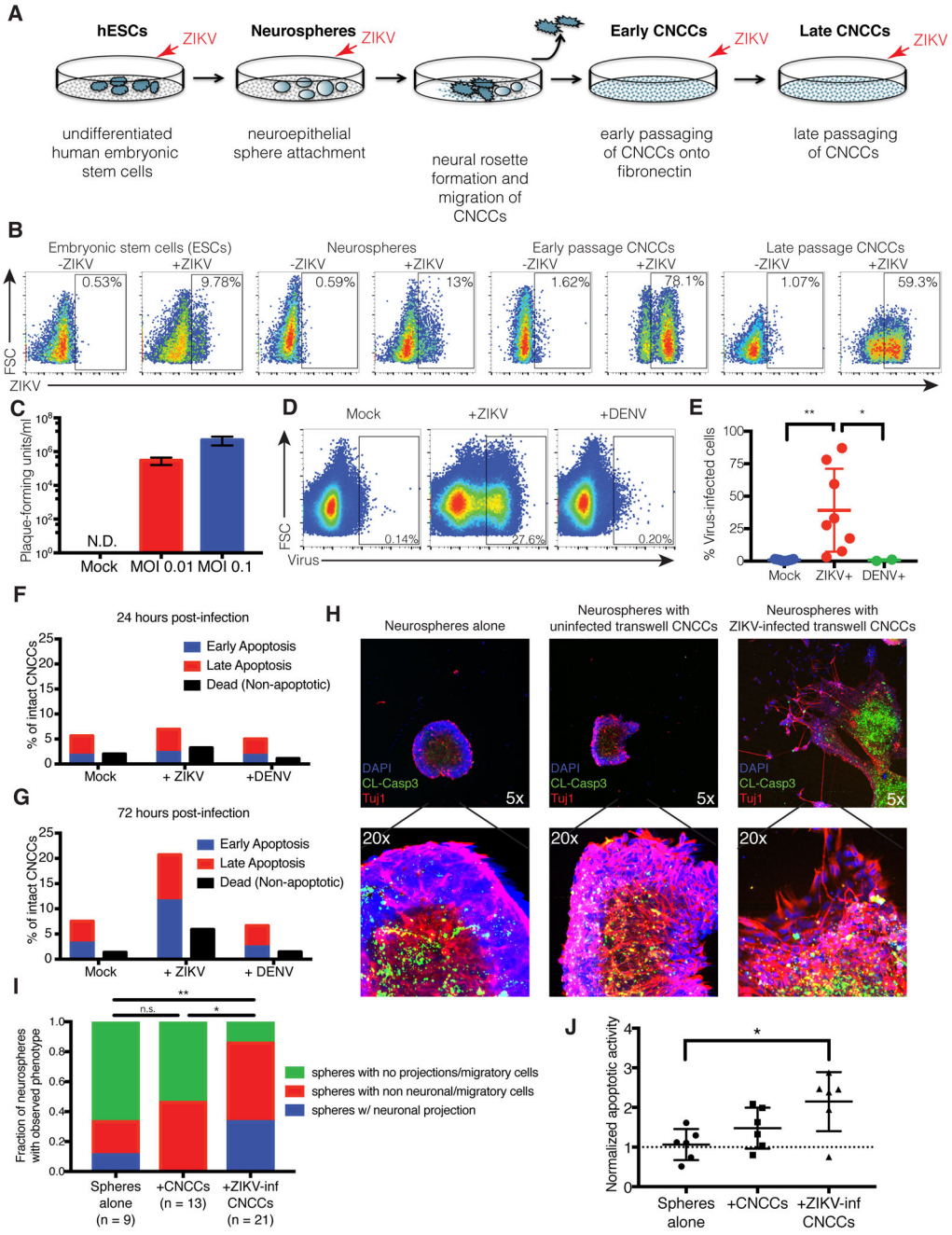

Figure 1. Zika virus (ZIKV) productively infects cranial neural crest cells (CNCCs)

A. Model of *in vitro* human neural development.

B. Embryonic stem cells (ESCs), neurospheres, and CNCCs were infected with ZIKV at MOI 0.1 (or mock infected in PBS) for 1 hour, and incubated for 23 hours at 37C. Infection was detected by intracellular staining for ZIKV with anti-flavivirus group surface antigen and analyzed by flow cytometry. See also Figure S1A.

C. Viral titers in culture supernatants as determined by plaque assay on Vero cells. Bars represent mean titer from two technical replicates of supernatants from two independent

biological experiments. Plaque formation was not detected (N.D.) in supernatants from mock-infected controls. Error bars are S.D.

D. CNCCs were infected with ZIKV or DENV at matched MOI (or mock infected in PBS) for 1 hour, followed by 23 hours of incubation at 37°C. Infection was detected by intracellular staining for ZIKV with anti-flavivirus group surface antigen and flow cytometry. Data is from a representative experiment.

E. Summary of infections of CNCCs. Points represent independent biological experiments. ZIKV vs. mock, p = 0.0078, Wilcoxon paired signed-rank test. ZIKV vs. DENV, p = 0.044, Mann-Whitney test. (Mock and ZIKV n=10, DENV n=2). *p < 0.05; **p < 0.01.

F–G. Quantifications of flow cytometry analysis of apoptotic death at 24 hours (F) and 72 hours (G) after infection. Cells were stained with Annexin V and propidium iodide to mark early apoptosis (Annexin V+/PI−), late apoptosis (Annexin V+/PI+) and non-apoptotic dead cells (Annexin V−/PI+). See also Figure S1E.

H. Confocal immunofluorescent images of neurospheres after 72 hours of transwell culture. Neurospheres were incubated alone (left), or with uninfected (center) and ZIKV-infected (right) CNCCs on the transwell membrane. Neurospheres were stained for cleaved caspase-3 (green), Tuj1 (red), and DAPI (blue). See Figure S1F for ZIKV-infected neurospheres alone.

i. Example of non-neuronal migratory cellular outgrowth

ii. Example of neuronal projections

I. Quantification of neurosphere morphology after exposure to transwell CNCCs. Spheres alone vs. +ZIKV-inf CNCCs, p = 0.0041, chi-squared test of equal proportions; uninfected CNCCs vs. ZIKV-inf CNCCs, p = 0.0139, chi-squared test of equal proportions. *p < 0.05; **p < 0.01.

J. Quantification of apoptotic activity in neurospheres. Confocal image z-stacks were analyzed for the intensity of Tuj1 and caspase signals. Caspase-3 intensities were normalized by Tuj1 signal (in the central bolus of the neurosphere) to account for differences in neurosphere size. Spheres alone vs. +ZIKV-inf CNCCs, p = 0.0260, Mann-Whitney test; uninfected CNCCs vs. ZIKV-inf CNCCs, p = 0.1320, Mann-Whitney test.
*p < 0.05.

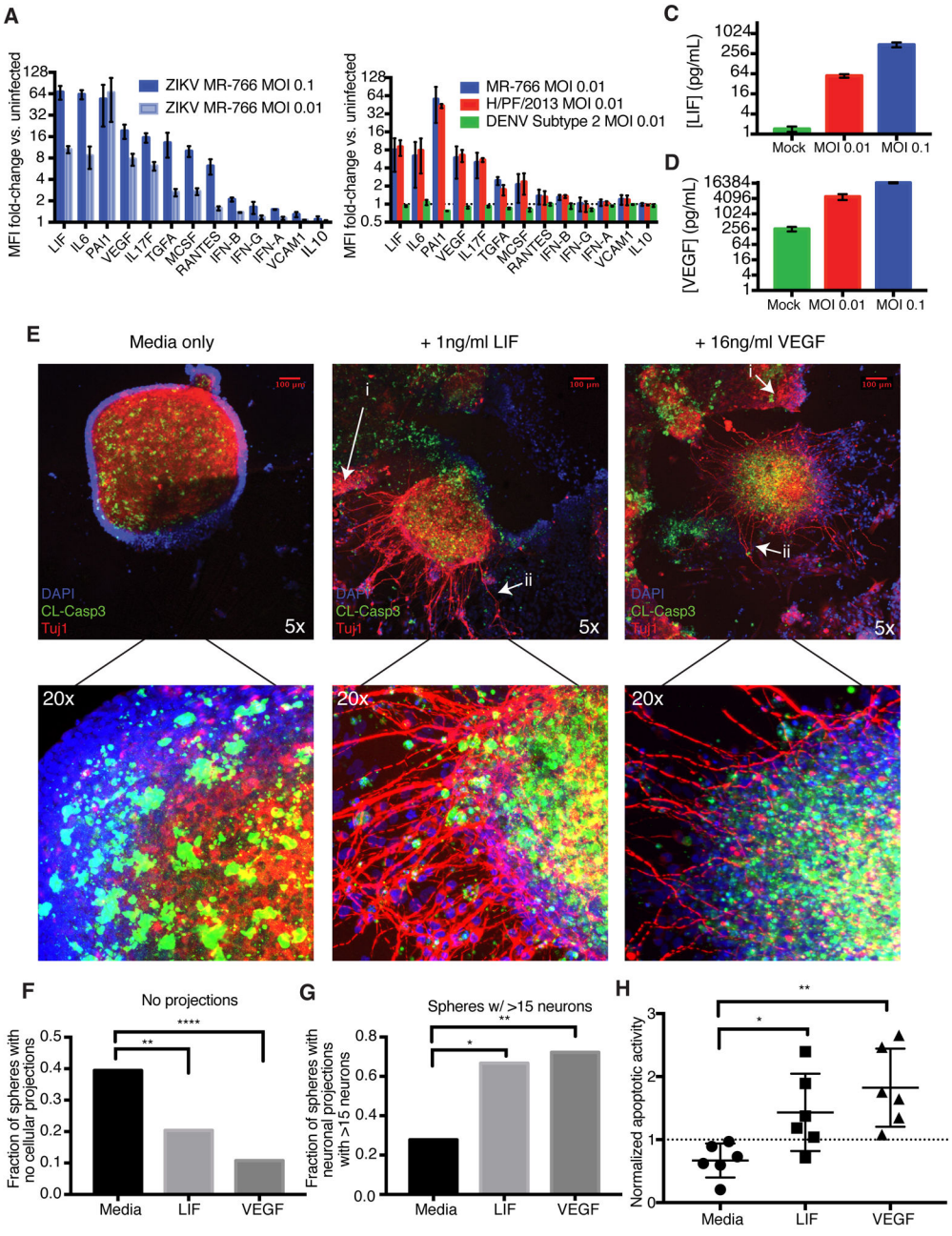

Figure 2. ZIKV-Infected CNCCs secrete LIF and VEGF at high concentrations, promoting apoptosis and premature neuronal formation in neurospheres

A. Cell culture supernatants were collected from CNCCs infected with ZIKV at MOI 0.1 or 0.01 or mock infected for 24 hours. Secreted cytokine levels were measured by a 63-plex Luminex assay. Shown here are analytes with >5-fold induction, IFNs, and VCAM1 and IL-10 for comparison. Data is represented as mean fluorescent intensity (MFI) fold-change compared to uninfected sample. Each bar represents mean MFI from two technical replicates from each of two independent biological experiments. Error bars represent S.D. See also Figure S2A.

B. Luminex fold-changes 24 hours after infection with MOI 0.01 ZIKV or DENV or mock infection. Data is represented as mean fluorescent intensity (MFI) fold-change compared to uninfected sample. Each bar represents mean MFI from two technical replicates from each of two independent biological experiments. Error bars represent S.D. See also Figure S2F.
C–D. Concentrations of (C) LIF and (D) VEGF in culture supernatants after 24 hour ZIKV infection at MOI 0.1, 0.01 or mock infection. Values represent mean concentration as determined from standard curves for each analyte. Error bars represent S.E.M. of two independent biological experiments with two technical replicates each. See also Figure S2B–E.
E. Neural precursor cells were differentiated from hESCs and grown as neurospheres. Seven days after sphere formation, exogenous LIF or VEGF was added to culture media, and spheres were observed for 3 days, followed by fixation and staining for DNA (DAPI, blue), apoptosis (cleaved caspase-3, green), and β-tubulin to mark neurons (Tuj1, red). Representative images are shown of neurospheres grown in culture media alone (left panel), with 1 ng/ml LIF (center panel), and with 16 ng/ml VEGF (right panel). See also Figure S2G.

i. Examples of non-neuronal migratory cellular outgrowth

ii. Examples of neuronal outgrowth

F. Images were scored by an objective observer for morphology. Data represents proportions of spheres showing no migratory cell projections or neuronal projections under normal media conditions and after the addition of LIF or VEGF. Chi-squared test of equal proportions. See also Figure S2H-I.
G. Images scored positive for neurons were grouped into spheres with low (<15) and high (<15) numbers of neurons. Chi-squared test of equal proportions. See also Figure S2J.
H. Quantification of apoptotic activity in neurospheres. Confocal image z-stacks were analyzed for the intensity of Tuj1 and caspase signals. Caspase-3 intensities were normalized by Tuj1 signal (in the central bolus of the neurosphere) to account for differences in neurosphere size. Mann-Whitney test.
*p < 0.05; **p < 0.01; ***p <0.001; ****p < 0.0001.